HOKKAIDO UNIVERSITY

Title	Water Reduction Photocathodes Based on Ru Complex Dyes Covered with a Conjugated Polymer Nanosheet
Author(s)	Shimamura, Taku; Kobayashi, Atsushi; Oaki, Yuya et al.
Citation	Energy & fuels, 36(19), 11559-11566 https://doi.org/10.1021/acs.energyfuels.2c00859
Issue Date	2022-10-06
Doc URL	https://hdl.handle.net/2115/90573
Rights	This document is the Accepted Manuscript version of a Published Work that appeared in final form in Energy & fuels, copyright c American Chemical Society after peer review and technical editing by the publisher. To access the final edited and published work see https://pubs.acs.org/articlesonrequest/AOR-T8K3YHF5BCIPYCA65732.
Type	journal article
File Information	Energy Fuels_36(19)_11559-11566.pdf



Hokkaido University Collection of Scholarly and Academic Papers : HUSCAP

Water reduction photocathodes based on Ru-complex dyes covered with a conjugated polymer nanosheet

Taku Shimamura,[a] Atsushi Kobayashi,[a] Yuya Oaki,[b] Masaki Yoshida,[a] Masako Kato[a†]*

[a]Department of Chemistry, Faculty of Science, Hokkaido University, North-10 West-8, Kita-ku, Sapporo 060-0810, Japan.

[b]Department of Applied Chemistry, Faculty of Science and Technology, Keio University, 3-14-1 Hiyoshi, Kohoku-ku, Yokohama 223-8522, Japan.

ABSTRACT. Water-splitting dye-sensitized photoelectrochemical cells are promising devices for resolving energy and environmental problems by producing H_2, a clean energy source, from water and sunlight. However, their performance is still limited because of dye desorption from the electrode and their weak light-absorption efficiency. In this study, we fabricated two water-reducing photocathodes—NiO|**RuCP**/BQPy and NiO|**RuCP**-Zr-**RuP**/BQPy—by combining the layer-by-layer formation of mono- (**RuCP**) and bi- (**RuCP** and **RuP** with Zr^{4+} cations) layer molecular films of Ru(II) dyes, respectively, on a p-type NiO substrate with the chemical vapor deposition of nanosheet catalyst based on BQPy organic polymer comprising benzoquinone and pyrrole moieties. These photocathodes produced H_2 under visible-light irradiation and a small electrical bias in a 0.1 M Na_2SO_4 aqueous solution (λ >420 nm, 65 mW cm^{-2}, E = −0.254 V vs. NHE, pH 3). Both the photocurrent value and amount of H_2 produced by the double-dye-layered NiO|**RuCP**-Zr-**RuP**/BQPy were smaller than those of NiO|**RuCP**/BQPy, probably because of the energy transfer inactivation between the Ru(II) dyes, which competes with the reductive quenching (i.e., electron injection) by NiO. Ru(II) dye desorption from the NiO|**RuCP**/BQPy photocathode was significantly reduced to approximately a third of that of NiO|**RuCP**, indicating that the deposited BQPy polymer improved the durability of the photocathode. The deposition of the BQPy polymer can be easily performed under mild conditions (60 °C in air); therefore, this technique shows great potential application for the construction of various types of dye-sensitized water-reducing photocathodes.

Introduction

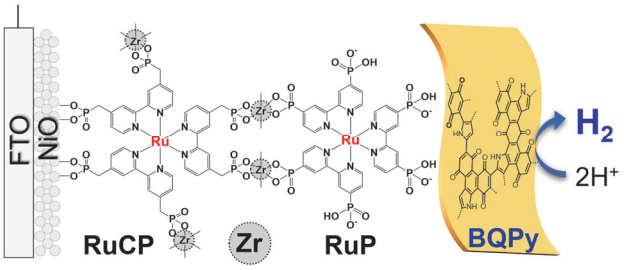
To overcome global warming and the energy crisis, H_2 production by solar water splitting has attracted considerable attention as a means of generating H_2 as a clean energy resource. Since water splitting by photoelectrochemical cells (PECs) comprising TiO_2 photoelectrodes was achieved by Honda and Fujishima,[1] many studies have been conducted to develop efficient water-splitting PEC systems.[2] One technical advantage of water-splitting PECs is the easy separation of H_2 and O_2, which are generated at spatially separated photocathodes and photoanodes, respectively.[3,4] In general, the three functional components—a light absorber, reduction catalyst that produces hydrogen, and an oxidation catalyst that produces oxygen—are essential to construct water-splitting PECs.[3] However, although various semiconductor materials have been developed to fulfill these requirements,[5-9] the construction of water-splitting PECs suitable for practical H_2 generation remains challenging.

Among the water-splitting PECs, dye-sensitized photoelectrochemical cells (DSPECs) composed of semiconductor electrodes and photosensitizing dyes are a promising approach for assembling the essential functions for the water-splitting reaction. This approach enables us to not only expand the visible light absorption ability based on the dye molecule, but to also investigate the photo/electrochemical behavior at the dye–semiconductor interface based on the response of the dye moelcules.[10-12] Taking advantage of these features, various photocathodes for H_2 evolution have been developed by combining photosensitizing dyes, molecular catalysts, and a typical p-type semiconductor NiO substrate that can be easily fabricated and quickly injects electrons into the photoexcited dye.[13,14] In recent years, several interesting approaches for functional assembly, ranging from the simple combination of co-adsorbed molecular dyes and catalysts[12,15-18] to the immobilization of supramolecular dyads acting as both the photosensitizer and catalyst[19-25] to the

coupling of surface-immobilized dyes and homogeneous molecular catalysts,[26-28] have been suggested as H_2-evolving photoelectrodes for water-splitting DSPEC. Further, the arrangement of the dye and catalyst molecules on the semiconductor surface has been successfully controlled using a layer-by-layer method.[29-32] These recent works indicate that the molecular assembly at the p-type semiconductor surface can offer wide designability for photoelectrochemical H_2 evolution. However, the activity and durability of these dye-sensitized H_2 evolution photocathodes are still limited, probably because of the easy desorption of dye molecules and back reactions at the semiconductor–dye–catalyst interfaces. The fabrication of dye-sensitized H_2-evolving photoelectrodes by not only the self-assembly of functional molecules, but also the integration of other functional materials may open a new avenue to overcome these issues. In this context, π-conjugated polymer catalysts, such as graphenes and carbon nitrile, are promising materials for H_2 evolution photocathodes because of their low overpotentials and high electric conductivities.[33-37] However, it is still challenging to integrate photosensitizing dyes and polymer catalysts because of the different sizes of the materials.

In this study, to overcome this issue, we have newly fabricated two H_2 evolution photocathodes, NiO|**RuCP**/BQPy and NiO|**RuCP**-Zr-**RuP**/BQPy, by the chemical vapor deposition of an organic nanosheet catalyst—a BQPy polymer containing benzoquinone (BQ) and pyrrole (Py) moieties[38]— and the layer-by-layer formation of mono- and bi-layer molecular films of Ru(II) dyes (**RuCP** = $[Ru(4,4'\text{-}(CH_2PO_3H_2)_2bpy)_3]Cl_2$ and **RuP** = $[Ru(4,4'\text{-}(PO_3H_2)_2)_2bpy)_3]Cl_2$) [29-32, 39-42] on a NiO electrode surface (Scheme 1). We also demonstrated that these BQPy-deposited photocathodes produce H_2 under visible-light irradiation with a small external electrical bias (λ >420 nm, 0.416 W cm^{-2}, E_{appl} = –0.254 V vs. NHE), and that the desorption of Ru(II) dyes is effectively suppressed by BQPy deposition. This catalyst-deposition

approach, which is based on easy and mild reaction conditions, is suitable for combination with thermally instable materials, such as functional molecules. Therefore, we believe that this strategy will open a new pathway for the preparation of highly active and durable photoelectrodes for water splitting DSPECs.



Scheme 1. Schematic structure of the NiO|**RuCP**-Zr-**RuP**/BQPy photocathode.

Results and Discussion

Preparation and characterization of the multilayered photocathodes

UV-vis diffuse reflectance and X-ray fluorescence (XRF) analyses were performed to confirm that the Ru dye was loaded on the NiO electrode (Figure 1). For the single dye-loaded photocathode NiO|**RuCP**, the ^{1}MLCT absorption band of **the RuCP** dye was observed at approximately 470 nm, indicating that the **RuCP** dye was successfully immobilized on the NiO surface by the phosphonate groups. The ^{1}MLCT absorption band was more intense for the double-dye-layered photocathode NiO|**RuCP**-Zr-**RuP**, suggesting that the loading amount of Ru(II) dye per unit surface area was increased by dye layering with the Zr^{4+}–phosphonate bonds. In the XRF spectra, the Kα and Kβ radiation of Ni was clearly observed at approximately 7.5 and 8.2 keV, respectively, for the NiO electrode, confirming that NiO was deposited on the fluorine-doped tin oxide (FTO) substrate (Figure 1b). The other photocathodes, namely NiO|**RuCP**, NiO|**RuCP**-Zr, and NiO|**RuCP**-Zr-**RuP**, exhibited weak but evident Ru Kα radiation at 19.2 keV (Figure 1c). The Ru Kα peak intensity of NiO|**RuCP**-Zr-**RuP** was stronger than those of NiO|**RuCP** and NiO|**RuCP**-Zr, suggesting an increase in the loading amount of Ru(II) dye, as revealed by the UV-vis diffuse reflectance spectra. The loading amounts of **RuCP** and **RuP** on the NiO electrode were estimated from the UV-vis absorption spectra of the supernatant solutions obtained after the immobilization reactions (Figure S1 and Table S1). A loading amount of 9.7 nmol per cm^2 was estimated for NiO|**RuCP**, which increased to 28.8 nmol per cm^2 for NiO|**RuCP**-Zr-**RuP**. This increase was attributed to the second immobilization of the **RuP** dye with the Zr^{4+}-phosphonate coordination bonds. Although the Zr K radiations were commonly observed for these photoelectrodes because of the Zr component in FTO glass, the Zr Kα and Kβ radiations of NiO|**RuCP**-Zr and NiO|**RuCP**-Zr-**RuP** were stronger than that of

electrodes without Zr^{4+} cation, NiO and NiO|**RuCP** (Figure S2). This result suggests that the Zr^{4+} cations were successfully immobilized by the phosphonate groups of **RuCP** to form the crosslinking sites for 2nd **RuP** dye layer formation.

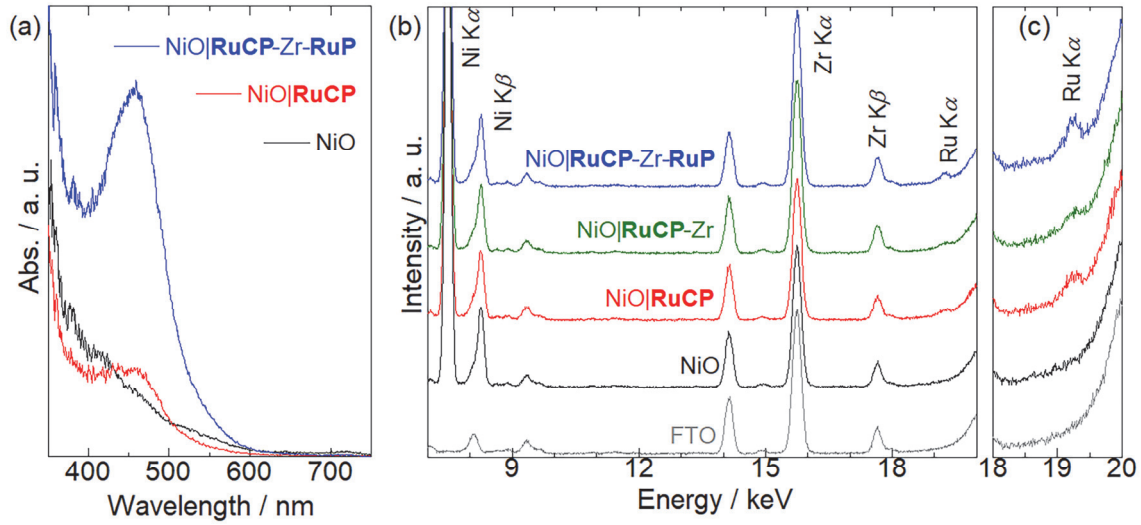


Figure 1. (a) UV-vis diffuse reflectance and (b) XRF spectra of NiO, NiO|**RuCP**, NiO|**RuCP**-Zr, and NiO|**RuCP**-Zr-**RuP** photocathodes at 293 K. (c) Magnification of the XRF spectra in the Ru Kα region. Spectra of the FTO substrate in (b) and (c) are illustrated in grey.

The surface-deposited BQPy polymer catalyst on NiO|**RuCP** and NiO|**RuCP**-Zr-**RuP** was next characterized by scanning electron microscopy (SEM). A porous particle structure with a diameter of approximately 4 μm was clearly observed for the NiO electrode (Figure 2a), confirming the formation of a porous NiO surface, as previously reported.[29, 43] The thickness of NiO was estimated to be about 4.5 μm by the cross-sectional SEM image (Figure S3), suggesting the suitable surface area for Ru(II)-dye sensitization. Near-identical porous particles were

observed for the double-dye-layered photocathode NiO|**RuCP**-Zr-**RuP** (Figure 2b), suggesting that the double layering of the **RuCP** and **RuP** dyes with Zr^{4+} cations had negligible effect on the surface NiO electrode structure. On the other hand, the surface scanning electron micrographs of NiO|**RuCP**/BQPy and NiO|**RuCP**-Zr-**RuP**/BQPy indicate that the surface of the NiO porous structure was covered by a thin film-like product (<1 μm thickness, Figures 2c and 2d), which was probably derived from the BQPy polymer. The IR spectra of NiO|**RuCP**/BQPy and NiO|**RuCP**-Zr-**RuP**/BQPy are very similar to those of the BQPy polymer (Figure S4). [38] These results clearly indicate that the thin BQPy polymer catalyst was successfully deposited on the surfaces of the NiO|**RuCP** and NiO|**RuCP**-Zr-**RuP** electrodes upon exposure to mixed BQ/Py vapor (see Experimental section for details).

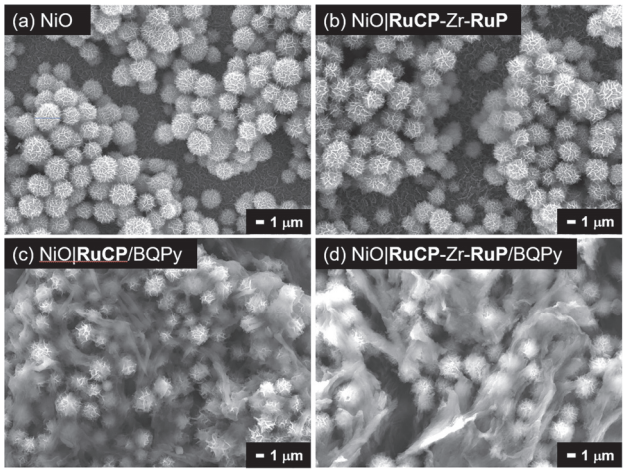


Figure 2. Surface scanning electron micrographs of the (a) NiO, (b) NiO|**RuCP**-Zr-**RuP**, (c) NiO|**RuCP**/BQPy, and (d) NiO|**RuCP**-Zr-**RuP**/BQPy electrodes. Each scale bar at the bottom right of the panels represents 1 μm.

Photoelectrochemical H_2 evolution

Photoelectrochemical measurements of the fabricated photoelectrodes were performed using Ag/AgCl and Pt coil as the respective reference and counter electrodes in 0.1 M Na_2SO_4 aqueous electrolyte solution (pH 3.0) at 293 K. The BQPy polymer catalysts of the NiO|**RuCP**/BQPy and NiO|**RuCP**-Zr-**RuP**/BQPy photocathodes were activated for the H_2 evolution reaction by photochemical reduction prior to these photoelectrochemical measurements (see Experimental section for details). Figure 3 shows the linear sweep voltammetry (LSV) results performed using chopped visible light irradiation (λ >420 nm, 0.416 W cm^{-2}, ON-OFF switching every 10 s) at a scan rate of 5 mV. All the Ru-dye-containing photoelectrodes—NiO|**RuCP**, NiO|**RuCP**-Zr-**RuP**, NiO|**RuCP**/BQPy, and NiO|**RuCP**-Zr-**RuP**/BQPy—exhibited cathodic photocurrents upon light irradiation, which was negligible for the pristine NiO electrode. This photocurrent was attributed to the electron flow from the NiO substrate to the photoexcited Ru dye present on the electrode surface. The single-layer photocathode NiO|**RuCP** presented a small anodic photocurrent in the positive potential region above +0.15 V and a relatively large cathodic photocurrent in the more negative potential region. This latter photocurrent was attributed to the reductive quenching of the excited **RuCP*** dye by the NiO substrate to form the one-electron reduced species **RuCP**$^{-}$, as reported by Reisner et al.[29] In fact, for the NiO|**RuCP** electrode, the ^{3}MLCT emission of the immobilized **RuCP** dye in the emission spectrum was negligible (Figure S5), which is consistent with the reductive quenching by NiO. On the other hand, the small anodic photocurrent observed in the positive potential region possibly originates from excited electron injection from the photoexcited **RuCP*** dye into the Ni^{3+} surface defect sites of the NiO electrode generated under positive potential bias. This is consistent with the disappearance of the reduction wave of the Ni^{3+} impurity sites[43,44] of the NiO electrode in the negative potential

region below +0.1 V, and correspondingly, the clear switching of the small anodic to the cathodic photocurrent.

The double-dye-layered photocathode NiO|**RuCP**-Zr-**RuP** also exhibited a cathodic photocurrent comparable to that of NiO|**RuCP** in the potential range of +0.1 to +0.4 V. As previously discussed, the immobilized amount of Ru dyes per unit area in NiO|**RuCP**-Zr-**RuP** was estimated to be approximately double that in NiO|**RuCP**; thus, the photoelectric conversion efficiency was approximately reduced to half by the double-layering of the Ru dyes. One of the possible origins is the energy transfer between the two different Ru dyes, **RuCP** and **RuP**, wherein the wavelength of the emission maximum of the former is shorter than that of the latter; this suggests energy transfer from the inner **RuCP** to the outer **RuP** dye as reported in several literature studies.[40,42] This energy transfer (< 200 ns)[40] may be competitive to the electron-injection process from NiO to **RuCP*** that should be slower than that to **RuP*** (<100 ps under applying the vias at –0.2 V)[45] because of the methyl-spacer between the phosphonate and bpy ligand, resulting in the lower photoelectric conversion efficiency. When **RuP*** is produced either by such an energy transfer from **RuCP** or by direct photoexcitation, the reductive quenching of **RuP*** by the NiO electrode is less efficient because of the long distance from the NiO surface via the **RuCP** dye and Zr^{4+} cations. In fact, the ^{3}MLCT emission for the NiO|**RuCP**-Zr-**RuP** electrode, was slightly observed at approximately 650 nm (Figure S5), suggesting less efficient reductive quenching by the NiO substrate. On the other hand, NiO|**RuCP**-Zr-**RuP** showed a comparable cathodic photocurrent even in the positive potential region above +0.15 V, in which NiO|**RuCP** showed a weak photoanodic current. Although the details are still under investigation, it is possible that the $ZrOCl_2$ used for the dye layering to prepare NiO|**RuCP**-Zr-**RuP** may react with the surface defects on the NiO electrode. Thus, the surface defects of the

NiO electrode can be eliminated by Zr^{4+}-trapping to prevent the formation of high-valent Ni sites.[44] This leads to a cathodic photocurrent from the NiO electrode to the photoexcited Ru dye even in the positive potential region.

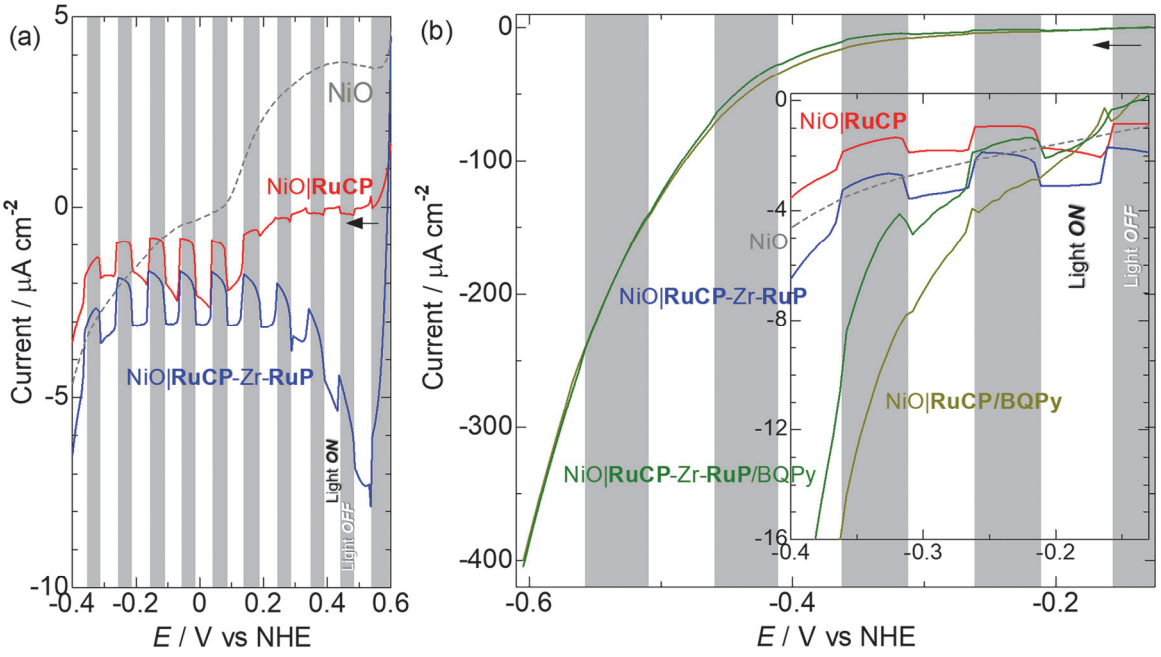


Figure 3. LSV scans of the (a) NiO (gray dashed lines), NiO|**RuCP** (red), and NiO|**RuCP**-Zr-**RuP** (blue) electrodes and (b) NiO|**RuCP**/BQPy (dark yellow) and NiO|**RuCP**-Zr-**RuP**/BQPy (green) electrodes. Conditions: Scan rate = 5 mV s^{-1}, chopped light irradiation (λ >420 nm, 0.416 W cm^{-2}), three-electrode setup with Ag/AgCl/KCl(sat.) reference and Pt coil counter electrodes, 0.1 M Na_2SO_4 (pH 3.0) aqueous solution, Ar atmosphere, and 293 K. Inset in (b) compares the magnification of the potential range from –0.4 to –0.15 V of the electrodes with and without BQPy. Gray backgrounds indicate the time duration without light irradiation.

Under dark conditions, both BQPy polymer-deposited photoelectrodes, NiO|**RuCP**/BQPy and NiO|**RuCP**-Zr-**RuP**/BQPy, exhibited remarkably larger cathodic currents, than did the

photoelectrodes without BQPy, in the negative potential region below −0.3 V vs NHE. These results suggest catalytic activity of the BQPy polymer toward H_2 evolution, as reported previously[38], even though the Ru-dye mono- or bilayer was incorporated between the NiO substrate and BQPy polymer. The cathodic currents of the BQPy-polymer-deposited photoelectrodes in this negative potential region were clearly enhanced by light irradiation, as shown in the LSV curves obtained under chopped light irradiation (inset of Figure 3b) and their comparison with those under dark and continuous light irradiation (Figure S6). This cathodic photocurrent at −0.3 V of NiO|**RuCP**/BQPy was lower than that of NiO|**RuCP** without BQPy polymer deposition. A plausible origin may be the energy transfer deactivation of **RuCP** by the BQPy catalyst, wherein the photoexcited **RuCP*** donates its excitation energy to the BQPy polymer catalyst before receiving an electron from the NiO substrate as suggested by the spectral overlap of the absorption of BQPy and emission of **RuCP** (Figure S7). On the other hand, such a decrease in the cathodic photocurrent by BQPy deposition was negligible for NiO|**RuCP**-Zr-**RuP**/BQPy. These contrasting results were attributed to the spatial separation of the **RuCP** dye from BQPy by the second **RuP** dye layer, leading to less efficient energy transfer quenching by BQPy.

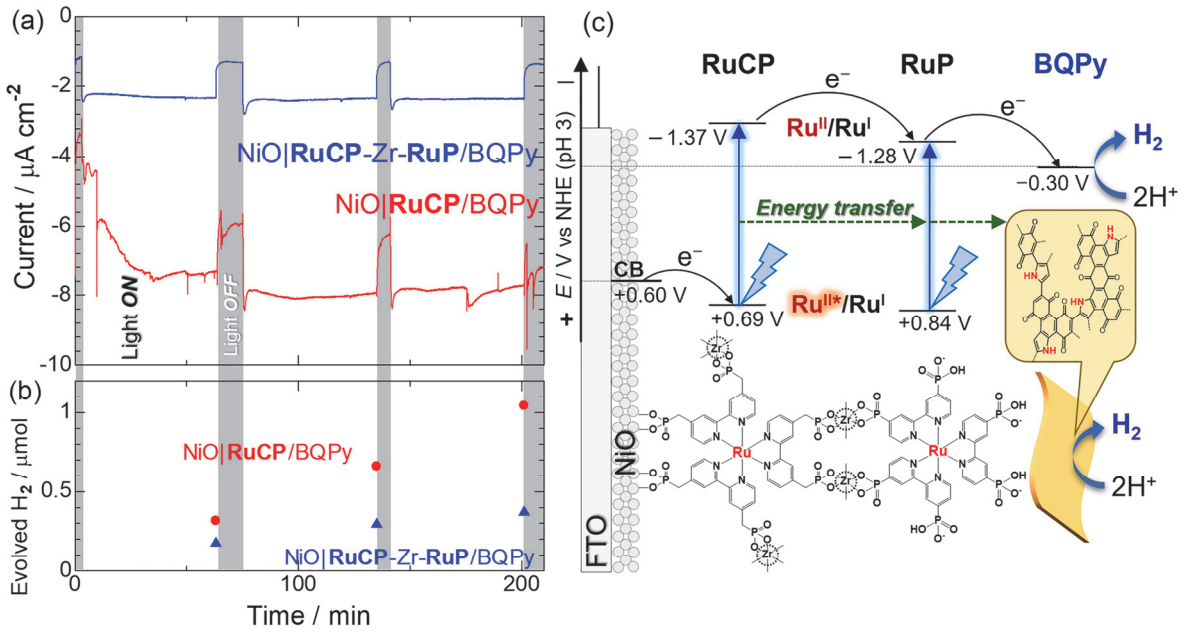


Figure 4. (a) Chronoamperometry of the NiO|**RuCP**/BQPy (red) and NiO|**RuCP**-Zr-**RuP**/BQPy (blue) photocathodes under chopped light irradiation at E_{appl} = −0.254 V vs NHE. (b) Evolved H_2 amount after every hour of irradiation estimated by GC analysis. All experiments were performed in a three-electrode setup with Ag/AgCl/KCl(sat.) reference and Pt coil counter electrodes, under Ar atmosphere, in 0.1M Na_2SO_4 (pH 3.0) aqueous solution, at 293 K. Gray backgrounds indicate the time duration without light irradiation. (c) Schematic energy diagram and layered structure of the NiO|**RuCP**-Zr-**RuP**/BQPy H_2-evolving photocathode. The redox potentials of Ru(II) dyes are approximated by the values of phosphonate-omitted analogues.[46]

Chronoamperometry measurements were conducted using BQPy polymer catalyst-deposited photocathodes—NiO|**RuCP**/BQPy and NiO|**RuCP**-Zr-**RuP**/BQPy—under chopped light irradiation (Hourly ON/OFF cycles under an applied bias E = –0.254 V vs NHE; Figure 4(a)). The cathodic photocurrent of NiO|**RuCP**/BQPy during the initial hour of irradiation was

unstable but gradually increased until a stable photocurrent |j| of approximately 2.13 μA cm^{-2} was observed in the second and third hours of irradiation. This unstable behavior in the initial 1 h might be due to the re-activation of partially deactivated BQPy polymer during the setup of the photoelectrochemical cell. In contrast, the double-dye-layered photoelectrode NiO|**RuCP**-Zr-**RuP**/BQPy showed a stable photocurrent (|j| ≈1.08 μA cm^{-2}) even in the initial hour of irradiation, which was estimated to be approximately half that of NiO|**RuCP**/BQPy. The stabler behavior of NiO|**RuCP**-Zr-**RuP**/BQPy than NiO|**RuCP**/BQPy implies that the thicker Ru(II) dye layer prevents the BQPy polymer catalyst from oxidative deactivation by NiO substrate under applying positive potential. This lower photocurrent of NiO|**RuCP**-Zr-**RuP**/BQPy was attributed to the energy transfer from the photoexcited **RuCP*** to **RuP,** which may compete with the reductive quenching by the NiO substrate, as previously discussed for the photoelectrodes without the BQPy polymer. In NiO|**RuCP**/BQPy, the photoexcitation of the **RuCP** dye should generate the one-electron-reduced **RuCP**$^{-}$ via reductive quenching by the NiO substrate. The redox potential (Ru^{II}/Ru^{I}) of the **RuCP**$^{-}$ species is sufficiently negative to donate the electron to BQPy (~ –0.3 V vs NHE),[47,48] resulting in hydrogen evolution by the catalytically active nitrogen sites in BQPy polymer.[38] In the case of NiO|**RuCP**-Zr-**RuP**/BQPy, the one-electron-reduced **RuCP**$^{-}$ donates an electron to the BQPy catalyst via the **RuP** dye, which has a more positive Ru^{II}/Ru^{I} redox potential than does **RuCP** (Figure 4(c)). Indeed, gas chromatography analysis of the gas phase of the photoelectrochemical cell clearly revealed that the estimated amounts of H_2 after three hours of irradiation were 1.043 ± 0.059 μmol for NiO|**RuCP**/BQPy and 0.370 ± 0.021 μmol for NiO|**RuCP**-Zr-**RuP**/BQPy (Figure 4(b)). These amounts qualitatively agree with the order of the cathodic photocurrent NiO|**RuCP**/BQPy > NiO|**RuCP**-Zr-**RuP**/BQPy. Notably, negligible H_2 was detected for the NiO|BQPy electrode without any Ru

dyes, even under the same experimental conditions. Thus, we supposed that the charge separation process at the NiO|**RuCP** interface plays an important role in the photoelectrochemical H_2 evolution reaction. Obtained SEM images of these photoelectrodes after the H_2 evolution reaction were similar to that before the reaction (Figure S8), suggesting the enough stability for at least several hours of photoelectrochemical H_2 evolution reaction.

To evaluate the effect of dye-layering and BQPy-polymer deposition on the photoelectrode stability, each photoelectrode—NiO|**RuCP**, NiO|**RuCP**-Zr-**RuP**, NiO|**RuCP**/BQPy, and NiO|**RuCP**-Zr-**RuP**/BQPy—was immersed in an electrolyte solution (pH 3.0, 0.1 M Na_2SO_4 aq) for one day under dark conditions, and the amount of desorbed Ru dye was quantified by UV-vis absorption spectroscopy (Figure 5, Table 1). The ^{1}MLCT absorption band derived from the Ru(II) dye was slightly observed for all the electrolyte solutions after immersion. The ^{1}MLCT absorption of the electrolyte solution in which NiO|**RuCP**-Zr-**RuP** was immersed was comparable to that of NiO|**RuCP**. This suggested that similar amounts of Ru dyes were desorbed, despite the Ru dye loading amount of NiO|**RuCP**-Zr-**RuP** being approximately triple that of NiO|**RuCP** (see Table 1). The different positions of the strong π–π* absorption band at approximately 295 nm indicated that not the inner **RuCP** dye but the outer **RuP** dye of the NiO|**RuCP**-Zr-**RuP** photoelectrode was predominantly desorbed. This probably occurred because the inner **RuCP** dye was effectively stabilized by coordination with the Zr^{4+} cation. In fact, ^{1}MLCT absorption for the electrolyte solution in which the Zr^{4+}-bound photoelectrode, NiO|**RuCP**-Zr, was immersed (Figure S9) was negligible. The ratio of desorbed to total amount of immobilized dye was estimated from the absorbance of the ^{1}MLCT transition at 66.0% for NiO|**RuCP** and 21.9% for NiO|**RuCP**-Zr-**RuP**, indicating that immobilization by Zr^{4+}-phosphonate coordination bonds is effective to suppress the desorption of the inner Ru dye.

Notably, the ^{1}MLCT absorption of the electrolyte solution in which NiO|**RuCP**/BQPy was soaked was significantly weaker than that for NiO|**RuCP**. This suggested that BQPy-polymer deposition on the NiO|**RuCP** photoelectrode surface is effective in preventing Ru-dye desorption. Indeed, the desorption ratio of the **RuCP** dye was reduced from 66.0% to 24.7% by covering the **RuCP** dye layer with the BQPy polymer. The BQPy polymer has a hydrophobic π-conjugated skeleton with hydrophilic OH groups coated on the **RuCP** dye layer so that the H_2 evolution reaction is possible in the hydrophilic cavity, while desorption of the dye is suppressed by the hydrophobic skeleton. The electrolyte solution in which NiO|**RuCP-**Zr-**RuP**/BQPy was immersed exhibited a broad absorption band extending to 700 nm, possibly originating from the BQPy polymer (Figure S9); this makes the estimation of the amount of desorbed Ru dye difficult. Such a desorption of the BQPy catalyst was negligible for NiO|**RuCP**/BQPy, suggesting that the double-layering of Ru(II) dyes by cross-linked Zr^{4+} cations may give a detrimental effect on the BQPy catalyst deposition.

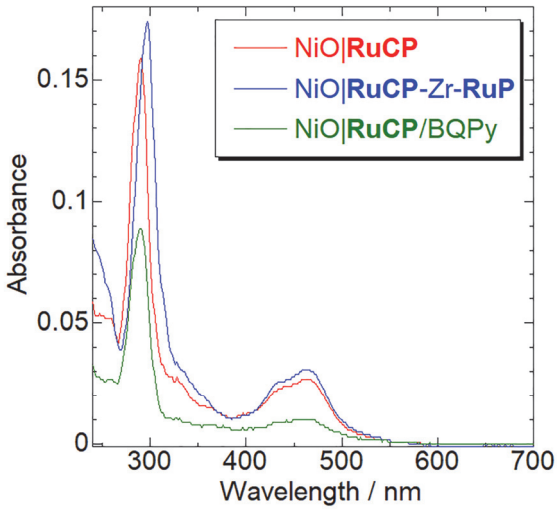


Figure 5. UV-vis absorption spectra of the electrolyte aqueous solutions (0.1 M Na_2SO_4 aq, pH 3.0) after one day immersion of the (red) NiO|**RuCP**, (blue) NiO|**RuCP**-Zr-**RuP**, and (green) NiO|**RuCP**/BQPy photocathodes at 293 K in air.

Table 1. Adsorbed (n_{ads}) and desorbed (n_{des}) amounts of Ru(II) dye for each photocathode.

Photocathode	n_{ads} (nmol cm^{-1})	Abs.[a]	n_{des} (nmol)[b]	Desorption ratio (%)
NiO|**RuCP**	9.7	0.027	6.4	66
NiO|**RuCP**/BQPy	9.7	0.010	2.4	24
NiO|**RuCP**-Zr-**RuP**	Total: 28.2 (**RuCP**: 9.7, **RuP**: 18.5)	0.031	6.3[c]	22

[a]Absorbance of the electrolyte solution at λ = 461 nm for **RuCP** and 463 nm for **RuP** after 24 h immersion of each photocathode (see Figure 5). [b]Estimated by the molar absorption coefficient (ε = 16900, 19600 for **RuCP** and **RuP**, respectively) and the solution volume (4 mL) used for UV-vis spectroscopy. [c]Desorbed dyes are mainly outer **RuP** dyes.

Conclusion

In this study, two dye-sensitized H_2 evolving photocathodes with an organic nanosheet catalyst, namely NiO|**RuCP**/BQPy and NiO|**RuCP**-Zr-**RuP**/BQPy, were constructed by chemical vapor deposition of a BQPy nanosheet catalyst coupled with layer-by-layer formation of mono- and bilayers of Ru(II) dye on the NiO substrate. These photocathodes successfully produced H_2 by visible-light irradiation, indicating that the developed polymer deposition approach is applicable for the preparation of H_2-evolving photocathodes. The results obtained for NiO|**RuCP**-Zr-**RuP**/BQPy indicate that the dye loading amount per unit area increased approximately threefold, compared to that of NiO|**RuCP**/BQPy, when using the layer-by-layer method. However, the photocurrent and hydrogen production were smaller than those of NiO|**RuCP**/BQPy, probably because the excitation energy transfer process of the two Ru(II) dyes competed with the photo-induced electron injection process from the NiO electrode. Ru dye desorption in the aqueous solution was effectively suppressed by the formation of a second **RuP** layer using Zr^{4+} cations and the deposition of the BQPy polymer. These results suggest that chemical vapor deposition of organic polymer catalysts on dye-sensitized photoelectrodes is a promising approach for water-reducing photocathodes based on both molecular and polymeric materials. Further study to overcome the energy transfer inactivation between Ru(II) dyes is in progress to construct more highly active and durable water-reduction photocathodes.

Experimental

Materials and methods

All commercially available starting materials, $Ni(NO_3)_2 \cdot 6H_2O$, hexamethylenetetramine, p-benzoquinone, and pyrrole (Wako Pure Chemical Industries) were used as received without further purification. **RuCP** and **RuP** were synthesized by a previously reported method.[48] The working electrode was prepared by cutting a fluorine-doped tin oxide (FTO)-coated glass plate (As One Corp., NPV-CFT2-7, R = 7Ω, 2.2 mm thickness) into 2.5 × 1 cm^2 slides. Nanostructured NiO was deposited on the FTO substrate as reported in the literature.[43]

Preparation of the Ru(II)-dye-sensitized NiO photoelectrodes

The **RuCP-**sensitized NiO photoelectrode, NiO|**RuCP**, was created by immersing the NiO electrode in a 50 μM **RuCP** aqueous solution overnight at 293 K, followed by washing with deionized water and EtOH, and finally drying in air. The second **RuP** immobilization was conducted as follows: The air-dried NiO|**RuCP** photoelectrode was immersed in a 5 mM $ZrOCl_2$/MeOH solution for 1 h at 293 K, washed with MeOH, and dried in air to afford the Zr^{4+}-bound electrode NiO|**RuCP**-Zr^{4+}. Finally, the obtained NiO|**RuCP**-Zr was immersed in a 50 μM **RuP** solution overnight at 293 K, washed with water and EtOH, and dried in air to afford the double-dye-layered NiO|**RuCP**-Zr-**RuP** photoelectrode. The obtained photoelectrodes were characterized by SEM, XRF, and UV-vis diffuse reflectance spectroscopy analyses.

Vapor deposition of the BQPy polymer catalyst

The BQPy polymer catalyst was deposited according to the literature[49] as follows: p-Benzoquinone powder (1.08 g, 10 mmol) and pyrrole (0.69 cm^3,10 mmol) were placed in two

different volume glass bottles. These monomer materials and the Ru(II)dye-sensitized NiO electrodes (NiO|**RuCP** or NiO|**RuCP**-Zr-**RuP**) were enclosed in a larger sealed vessel and heated at 60 °C for 100 min to afford the two BQPy-deposited photocathodes, NiO|**RuCP**/BQPy and NiO|**RuCP**-Zr-**RuP**/BQPy, which were then characterized by SEM and IR analysis.

Photoelectrochemistry

Electrochemical measurements were performed using an HZ-3000 potentiostat (Hokuto Denko) with three electrodes placed in an electrolysis cell (VB12A, EC Frontier) equipped with quartz glass for the photoelectrochemical measurements. Dye-sensitized NiO electrodes (1 cm^2 surface area), a Pt coil, and Ag/AgCl/KCl (sat.) were used as the working, counter, and reference electrodes, respectively, in 0.1 M Na_2SO_4 aqueous electrolyte solution (pH 3). All electrolyte solutions were purged by Ar bubbling for at least 20 min to remove any dissolved O_2. Photoelectrochemical measurements were performed using a xenon light source (MAX-303, Asahi Spectra) under visible light irradiation (>420 nm, 35 mW) from the back (FTO) side of the working electrode. Evolved H_2 present in the gas phase of the electrolysis cell was detected using a gas chromatography system (GC-14B, Shimadzu Inc.) equipped with an MS-5A column and a thermal conductivity detector.

Activation of the BQPy polymer catalyst by photoelectrochemical reduction

The BQPy polymer catalyst deposited on the surfaces of NiO|**RuCP**/BQPy and NiO|**RuCP**-Zr-**RuP**/BQPy was activated by photoelectrochemical reduction under visible light irradiation (>420 nm) and constant bias (E_{appl} = −0.5 V vs NHE) for application to the H_2 evolution reaction.[38] The efficiency of the BQPy polymer reduction was affected by the thickness of the Ru(II) dye layer, and thus, a constant photocurrent was obtained after 5 h and 7 h reaction for NiO|**RuCP**/BQPy

and NiO|**RuCP**-Zr-**RuP**/BQPy, respectively. These photoelectrochemically reduced photocathodes displayed a distinct catalytic current in the LSV measurements, under dark conditions, together with a significant decrease in the overpotential for H_2 evolution (Figure S9). These results indicated that the surface-deposited BQPy catalyst was sufficiently reduced to be activated for the H_2 evolution reaction.

ASSOCIATED CONTENT

Supporting Information. UV-Vis absorption spectra of the supernatant solutions obtained in the Ru(II) dye immobilizations; XRF spectra of Zr K region; Cross-sectional SEM image of NiO-FTO electrode; ATR-IR, excitation, and emission spectra of Ru(II) dye sensitized NiO photoelectrodes; LSV scans of NiO|**RuCP**/BQPy and NiO|**RuCP**-Zr-**RuP**/BQPy photoelectrodes under dark, chopped light, and continuous light irradiation; SEM images of NiO|**RuCP**/BQPy and NiO|**RuCP**-Zr-**RuP**/BQPy photoelectrodes after photoelectrochemical H_2 evolution reaction; UV-vis absorption spectra of the electrolyte aqueous solutions after 24 h immersion of Ru(II) dye sensitized NiO photoelectrodes. This material is available free of charge on the Internet at http://pubs.acs.org.

AUTHOR INFORMATION

Corresponding Author

*E-mail: akoba@sci.hokudai.ac.jp (A.K.)

Present Addresses

†Present address: Department of Applied Chemistry for Environment, School of Biological and Environmental Sciences, Kwansei Gakuin University, 2-1 Gakuen, Sanda, Hyogo 669-1337, Japan

Author Contributions

The manuscript was written through the contributions of all the authors. All the authors have approved the final version of the manuscript.

Funding Sources

This study was supported by the ENEOS Hydrogen Trust Fund, Casio Science Promotion Foundation and JSPS KAKENHI, Grant Numbers JP18K19086, JP17H06367, and JP20H05082.

ACKNOWLEDGMENTS

The authors thank Mr. N. Yoshimura (Hokkaido Univ.) for valuable support for SEM-EDS analysis.

REFERENCES

(1) Fujishima, A.; Honda. K. Electrochemical Photolysis of Water at a Semiconductor Electrode. *Nature* **1972**, *238*, 37–38.

(2) Yun, S.; Vlachopoulos, N.; Qurashi, A.; Ahmad, S.; Hagfeldt, A. Dye Sensitized Photoelectrolysis Cells. *Chem. Soc. Rev.* **2019**, *48*, 3705–3722.

(3) Yu, Z.; Li, F.; Sun, L. Recent Advances in Dye-Sensitized Photoelectrochemical Cells for Solar Hydrogen Production Based on Molecular Components. *Energy Environ. Sci.* **2015**, *8*, 760–775.

(4) Willkomm, J.; Orchard, K. L.; Reynal, A.; Pastor, E.; Durrant, J. R.; Reisner, E. Dye-Sensitised Semiconductors Modified with Molecular Catalysts for Light-Driven H_2 Production. *Chem. Soc. Rev.* **2016**, *45*, 9–23.

(5) Sivula, K.; Le Formal, F.; Grätzel, M. Solar Water Splitting: Progress Using Hematite (α-Fe_2O_3) Photoelectrodes. *ChemSusChem* **2011**, *4*, 432–449.

(6) Kalanur, S. S.; Duy, L. T.; Seo, H. Recent Progress in Photoelectrochemical Water Splitting Activity of WO_3 Photoanodes. *Top. Catal.* **2018**, *61*, 1043–1076.

(7) Park, Y.; McDonald, K. J.; Choi, K.-S. Progress in Bismuth Vanadate Photoanodes for Use in Solar Water Oxidation. *Chem. Soc. Rev.* **2013**, *42*, 2321–2337.

(8) Nann, T.; Ibrahim, S. K.; Woi, P. M.; Xu, S.; Ziegler, J.; Pickett, C. J. Water Splitting by Visible Light: A Nanophotocathode for Hydrogen Production. *Angew. Chem. Int. Ed.* **2010**, *49*, 1574–1577.

(9) Wick, R.; Tilley, S. D. Photovoltaic and Photoelectrochemical Solar Energy Conversion with Cu_2O. *J. Phys. Chem. C* **2015**, *119*, 26243– 26257.

(10) Ashford, D. L.; Gish, M. K.; Vannucci, A. K.; Brennaman, M. K.; Templeton, J. L.; Papanikolas, J. M.; Meyer, T. J. Molecular Chromophore–Catalyst Assemblies for Solar Fuel Applications. *Chem. Rev.* **2015**, *115*, 13006–13049.

(11) Wang, D.; Fei, L.; Huang Z.; Meyer, T. J. Design and Characterization of Surface Molecular Assemblies for the Preparation of Solar Fuels. *Chem. Phys. Rev.* **2022**, *3*, 011301.

(12) Li, F.; Fan, K.; Xu, B.; Gabrielsson, E.; Daniel, Q.; Li, L.; Sun, L. Organic Dye-Sensitized Tandem Photoelectrochemical Cell for Light Driven Total Water Splitting. *J. Am. Chem. Soc.* **2015**, 137, 9153–9159.

(13) Nikolaou, V.; Charisiadis, A.; Charalambidis, G.; Coutsolelos, A. G.; Odobel, F. J. Recent Advances and Insights in Dye-Sensitized NiO Photocathodes for Photovoltaic Devices. *J. Mater. Chem. A* **2017**, *5*, 21077–21113.

(14) Wood, C. J.; Summers, G. H.; Clark, C. A.; Kaeffer, N.; Braeutigam, M.; Carbone, L. R.; D'Amario, L.; Fan, K.; Farré, Y.; Narbey, S.; Oswald, F.; Stevens, L. A.; Parmenter, C. D. J.; Fay, M. W.; La Torre, A.; Snape, C. E.; Dietzek, B.; Dini, D.; Hammarstrom, L.; Pellegrin, Y.; Odobel, F.; Sun, L.; Artero, V.; Gibson, E. A. A Comprehensive Comparison of Dye-Sensitized NiO Photocathodes for Solar Energy Conversion. *Phys. Chem. Chem. Phys.* **2016**, *18*, 10727– 10738.

(15) Fan, K.; Li, F.; Wang, L.; Daniel, Q.; Gabrielsson, E.; Sun, L. Pt-free Tandem Molecular Photoelectrochemical Cells for Water Splitting Driven by Visible Light. *Phys. Chem. Chem. Phys.* **2014**, *16*, 25234–25240.

(16) Antila, L. J.; Ghamgosar, P.; Maji, S.; Tian, H.; Ott, S.; Hammarström, L. Dynamics and Photochemical H_2 Evolution of Dye–NiO Photocathodes with a Biomimetic FeFe-Catalyst. *ACS Energy Lett.* **2016**, *1*, 1106–1111.

(17) Creissen, C. E.; Warnan, J.; Reisner, E. Solar H_2 Generation in Water with a $CuCrO_2$ Photocathode Modified with an Organic Dye and Molecular Ni Catalyst. *Chem. Sci.* **2018**, *9*, 1439–1447.

(18) Kaeffer, N.; Windle, C. D.; Brisse, R.; Gablin, C.; Leonard, D.; Jousselme, B.; Chavarot-Kerlidou, M.; Artero, V. Insights into the Mechanism and Aging of a Noble-Metal Free H2-Evolving Dye-Sensitized Photocathode, *Chem. Sci.* **2018**, *9*, 6721–6738.

(19) Ji, Z.; He, M.; Huang, Z.; Ozkan, U.; Wu, Y. Photostable p-Type Dye-Sensitized Photoelectrochemical Cells for Water Reduction. *J. Am. Chem. Soc.* **2013**, *135*, 11696–11699.

(20) Kaeffer, N.; Massin, J.; Lebrun, C.; Renault, O.; Chavarot-Kerlidou, M.; Artero, V. Covalent Design for Dye-Sensitized H_2-Evolving Photocathodes Based on a Cobalt Diimine-Dioxime Catalyst. *J. Am. Chem. Soc.* **2016**, *138*, 12308–12311.

(21) Pati, P. B.; Zhang, L.; Philippe, B.; Fernández-Terán, R.; Ahmadi, S.; Tian, L.; Rensmo, H.; Hammarström, L.; Tian, H. Insights into the Mechanism of a Covalently Linked Organic Dye–Cobaloxime Catalyst System for Dye-Sensitized Solar Fuel Devices. *ChemSusChem* **2017**, *10*, 2480–2495.

(22) Lyu, S.; Massin, J.; Pavone, M.; Muñoz-García, A. B.; Labrugère, C.; Toupance, T.; Chavarot-Kerlidou, M.; Artero, V.; Olivier, C. H_2-Evolving Dye-Sensitized Photocathode Based on a Ruthenium–Diacetylide/Cobaloxime Supramolecular Assembly. *ACS Appl. Energy Mater.* **2019**, *2*, 4971–4980.

(23) Huang, J.; Sun, J.; Wu, Y.; Turro, C. Dirhodium(II,II)/NiO Photocathode for Photoelectrocatalytic Hydrogen Evolution with Red Light. *J. Am. Chem. Soc.* **2021**, *143*, 1610–1617.

(24) Giannoudis, E.; Bold, A.; Müller, C.; Schwab, A.; Bruhnke, J.; Queyriaux, N.; Gablin, C.; Leonard, D.; Saint-Pierre, C.; Gasparutto, D.; Aldakov, D.; Kupfer, S.; Artero, V.; Dietzek, B.; Chavarot-Kerlidou, M. Hydrogen Production at a NiO Photocathode Based on a Ruthenium Dye–Cobalt Diimine Dioxime Catalyst Assembly: Insights from Advanced Spectroscopy and Post-Operando Characterization. *ACS Appl. Mater. Interfaces* **2021**, *13*, 49802–49815.

(25) Põldme, N.; O'Reilly, L.; Fletcher, I.; Portoles, J.; Sazanovich, I. V.; Towrie, M.; Long, C.; Vos, J. G.; Pryce, M. T.; Gibson, E. A. Photoelectrocatalytic H_2 Evolution from Integrated Photocatalysts Adsorbed on NiO. *Chem. Sci.* **2019**, 10, 99–112.

(26) Li, L.; Duan, L.; Wen, F.; Li, C.; Wang, M.; Hagfeldt, A.; Sun, L. Visible Light Driven Hydrogen Production from a Photo-Active Cathode Based on a Molecular Catalyst and Organic Dye-Sensitized p-Type Nanostructured NiO. *Chem. Commun.* **2012**, *48*, 988–990.

(27) Kamire, R. J.; Majewski, M. B.; Hoffeditz, W. L.; Phelan, B. T.; Farha, O. K.; Hupp, J. T.; Wasielewski, M. R. Photodriven Hydrogen Evolution by Molecular Catalysts Using Al_2O_3-Protected Perylene-3,4-Dicarboximide on NiO Electrodes. *Chem. Sci.* **2017**, *8*, 541–549.

(28) Click, K. A.; Beauchamp, D. R.; Huang, Z.; Chen, W.; Wu, Y. Membrane-Inspired Acidically Stable Dye-Sensitized Photocathode for Solar Fuel Production. *J. Am. Chem. Soc.* **2016**, *138*, 1174–1179.

(29) Gross, M. A.; Creissen, C. E.; Orchard, K. L.; Reisner, E. Photoelectrochemical Hydrogen Production in Water using a Layer-by-Layer Assembly of a Ru Dye and Ni Catalyst on NiO. *Chem. Sci.* **2016**, *7*, 5537–5546.

(30) Wang, D.; Sheridan, M. V.; Shan, B.; Farnum, B. H.; Marquard, S. L.; Sherman, B. D.; Eberhart, M. S.; Nayak, A.; Dares, C. J.; Das, A. K.; Bullock, R. M.; Meyer, T. J. Layer-by-Layer Molecular Assemblies for Dye-Sensitized Photoelectrosynthesis Cells Prepared by Atomic Layer Deposition. *J. Am. Chem. Soc.* **2017**, *139*, 14518–14525.

(31) Shan, B.; Sherman, B. D.; Klug, C. M.; Nayak, A.; Marquard, S. L.; Liu, Q.; Bullock, R. M.; Meyer, T. J. Modulating Hole Transport in Multilayered Photocathodes with Derivatized p-Type Nickel Oxide and Molecular Assemblies for Solar-Driven Water Splitting. *J. Phys. Chem. Lett.* **2017**, *8*, 4374–4379.

(32) Shan, B.; Das, A. K.; Marquard, S.; Farnum, B. H.; Wang, D.; Bullock, R. M.; Meyer, T. J. Photogeneration of Hydrogen from Water by a Robust Dye-Sensitized Photocathode. *Energy Environ. Sci.* **2016**, *9*, 3693–3697.

(33) Zheng, Y.; Jiao, Y.; Zhu, Y.; Li, L. H.; Han, Y.; Chen, Y.; Du, A.; Jaroniec, M.; Qiao, S. Z. Hydrogen Evolution by a Metal-Free Electrocatalyst. *Nat. Comm.* **2014**, *5*, 3783.

(34) Duan, J.; Chen, S.; Jaroniec, M.; Qiao, S. Z. Porous C_3N_4 Nanolayers@N-Graphene Films as Catalyst Electrodes for Highly Efficient Hydrogen Evolution. *ACS Nano* **2015**, *9*, 931–940.

(35) Chherti, M.; Maitra, S.; Chakraborty, H.; Waghmare, U. V.; Rao, C. N. R. Superior Performance of Borocarbonitrides, $B_xC_yN_z$, as Stable, Low-Cost Metal-Free Electrocatalysts for the Hydrogen Evolution Reaction. *Energy Environ. Sci.* **2016**, *9*, 95–101.

(36) Patra, B. C.; Khilari, S.; Manna, R. N.; Mondal, S.; Pradhan, D.; Pradhan, A.; Bhaumik, A. A Metal-Free Covalent Organic Polymer for Electrocatalytic Hydrogen Evolution. *ACS Catal.* **2017**, *7*, 6120–6127.

(37) Wang, H.; Li, X.-B.; Gao, L.; Wu, H.-L.; Yang, J.; Cai, L.; Ma, T.-B.; Tung, C.-H.; Wu, L.-Z.; Yu, G. Three-Dimensional Graphene Networks with Abundant Sharp Edge Sites for Efficient Electrocatalytic Hydrogen Evolution. *Angew. Chem. Int. Ed.* **2018**, *57*, 192-197.

(38) Yano; K. Sato; J. Suzuk; H. Imai; Y. Oaki Amorphous 2D Materials Containing a Conjugated-Polymer Network. *Comn. Chem.* **2019**, *2*, 97–105.

(39) Lee, H.; Kepley, L. J.; Hong, H. G.; Mallouk, T. E. Inorganic Analogs of Langmuir-Blodgett Films: Adsorption of Ordered Zirconium 1,10-Decanebisphosphonate Multilayers on Silicon Surfaces. *J. Am. Chem. Soc.* **1988**, *110*, 618–620.

(40) Hanson, K.; Torelli, D. A.; Vannucci, A. K.; Brennaman, M. K.; Luo, H.; Alibabaei, L.; Song, W.; Ashford, D. L.; Norri, M. R.; Glasson, C. R. K.; Concepcion, J. J.; Meyer, T. J. Self-Assembled Bilayer Films of Ruthenium(II)/Polypyridyl Complexes through Layer-by-Layer Deposition on Nanostructured Metal Oxides. *Angew. Chem. Int. Ed.* **2012**, *51*, 12782– 12785.

(41) Ding, X.; Gao, Y.; Zhang, L.; Yu, Z.; Liu, J.; Sun, L. Visible Light-Driven Water Splitting in Photoelectrochemical Cells with Supramolecular Catalysts on Photoanodes. *ACS Catal.* **2014**, *4*, 2347–2350.

(42) Yoshimura, N.; Kobayashi, A.; Yoshida, M.; Kato, M. Enhancement of Photocatalytic Activity for Hydrogen Production by Surface Modification of Pt-TiO_2 Nanoparticles with a Double Layer of Photosensitizers. *Chem. Eur. J.* **2020**, *26*, 16939–16946.

(43) Xi, Y. Y.; Li, D; Djurišić, A. B.; Xie, M. H.; Man, K. Y. K.; Chan, W. K. Hydrothermal Synthesis vs Electrodeposition for High Specific Capacitance Nanostructured NiO Films. *Electrochem. Solid-State Lett.* **2008**, *11*, D56–D59.

(44) Taggart, A. D.; Evans, J. M.; Li, L.; Lee, K. J.; Dempsey, J. L.; Kanai, Y.; Cahoon, J. F. Enabling Aqueous NiO Photocathodes by Passivating Surface Sites that Facilitate Proton-Coupled Charge Transfer. *ACS Appl. Energy Mater.* **2020**, *3*, 10702–10713.

(45) Dillon, R. J.; Alibabaei, L.; Meyer, T. J.; Papanikolas, J. M. Enabling Efficient Creation of Long-Lived Charge-Separation on Dye-Sensitized NiO Photocathodes, *ACS Appl. Mater. Interfaces* **2017**, *9*, 26786–26796.

(46) The redox potentials of **RuCP** and **RuP** were approximated by the values of analogue complexes without the phosphonate groups, $[Ru(4,4'\text{-dimethyl-}2,2'\text{-bipyridine})_3]^{2+}$ and $[Ru(2,2'\text{-bipyridine})_3]^{2+}$, respectively, reported in the following literature, because of the poor solubility to non-aqueous solvents.; Juris, A.; Balzani, V.; Barigelletti, F.; Campagna, S.; Belser, P.; Zelewsky, A. V. Ru(II) Polypyridine Complexes: Photophysics, Photochemistry, Electrochemistry, and Chemiluminescence, *Coord. Chem. Rev.* **1988**, *84*, 85-277.

(47) Zigler, D. F.; Morseth, Z. A.; Wang, L.; Ashford, D. L.; Brennaman, M. K.; Grumstrup, E. M.; Brigham, E. C.; Gish, M. K.; Dillon, R. J.; Alibabaei, L.; Meyer, G. J.; Meyer, T. J.; Papanikolas, J. M. Disentangling the Physical Processes Responsible for the Kinetic

Complexity in Interfacial Electron Transfer of Excited Ru(II) Polypyridyl Dyes on TiO_2. *J. Am. Chem. Soc.* **2016**, *138*, 4426-4438.

(48) Ashford, D. L.; Brennaman, M. K.; Brown, R. J.; Keinan, S.; Concepcion, J. J.; Papanikolas, J. M.; Templeton, J. L.; Meyer, T. J. Varying the Electronic Structure of Surface-Bound Ruthenium(II) Polypyridyl Complexes. *Inorg. Chem.* **2015**, *54*, 460-469.

(49) Kuwabara, K.; Masaki, H.; Imai, H.; Oaki, Y. Substrate Coating by Conductive Polymers through Spontaneous Oxidation and Polymerization. *Nanoscale* **2017**, *9*, 7895–7900.

Table of Contents graphic

